17A-04

APPLICATION OF CLUTTER POLYGONS IN TERMINAL DOPPLER WEATHER RADAR FOR IMPROVING THE DETECTION OF TERRAIN-INDUCED WINDSHEAR IN HONG KONG

Tse Shuk-mei* and Chan Ying-wa
Hong Kong Observatory, Hong Kong, China

1. Introduction

In 1996, the Hong Kong Observatory (HKO) installed its first Terminal Doppler Weather Radar (TDWR) at Tai Lam Chung (TLC) for detecting hazardous weather, including windshear and microbursts associated with convective storms, to support the operation of the Hong Kong International Airport (HKIA) (Lee and Shun 1998).

The HKIA is one of the busiest airports in the world and there were around 428,000 air traffic movements in 2018 (HKIA 2019). With a runway height of less than 10 m above the mean sea level (AMSL), the HKIA is geographically situated to the north of the hilly Lantau Island with mountains reaching around 900 m AMSL. To the north of the HKIA lies another mountain called Castle Peak which is as high as 600 m AMSL. In 2006, tourist cable cars started operation on the Lantau Island with a ropeway of about 5.7 km long (Figure 1).

From July 1998 to December 2009, about 1 in 500 flights arriving at or departing from the HKIA have reported significant windshear (windshear magnitude ≥ 7.7 ms^{-1} or 15 knots) (HKO 2010). Terrain-induced windshear is a major type of low-level windshear at the HKIA, accounting for about 70% of all pilot windshear reports (Shun and Chan 2008). It occurs predominantly in the late Spring season and may be caused by different types of airflow which tend to have a high spatial and temporal variability. These include reverse flows in mountain wakes (Shun and Lau 2000), wind jets emerging from the various gaps of the Lantau Island (Lau and Shun 2002), and vortices shedding from lee slopes of mountains (Shun et al. 2003), etc. All these terrain-induced features might propagate to the AREas Noted for Attention (ARENA) of the HKIA runways (Li et al. 2017) and affect the safety of aircraft taking off or landing at the runways.

In 2014, HKO installed a new TDWR at Brothers Point (BP), about 1 km east-southeast of the aging TLC TDWR which then served as the backup system in the provision of the windshear and microburst alerting services. Since the operation of the BP TDWR in April 2015, cases of over-warning of windshear were observed including (i) anomalous windshear or microburst alerts possibly caused by reverse flows in the wakes of Lantau mountains resulting in significantly higher alert values compared with human truthing; and (ii) strong sidelobe return echoes due to transit of marine vessels near the HKIA.

In 2016-2018, HKO experimented the use of clutter polygons and fine-tuned the BP TDWR's windshear and microbursts detection algorithm (WMDA) parameters for improving the over-warning problem. This paper describes the data, methodology and verification used in the experiment. The comparison results of the effectiveness of terrain-induced windshear detection between the new and the original BP TDWR settings are presented.

2. TDWR operation

2.1 Radar hardware and scanning modes

Both TLC and BP TDWRs are C-band radars with similar hardware specifications (Table 1). For each of the radar, it is equipped with dual transmitters, receivers and signal

* *Corresponding author address:* Tse Shuk-mei, Hong Kong Observatory, 134A Nathan Road, Hong Kong; email: smtse@hko.gov.hk.

processors to provide redundancy for enhancing operation. There are two scanning modes. The monitor mode is for general weather monitoring in a 5-minute volume scan. The scanning turns to hazardous mode when there is inclement weather. Scanning at 0.6°, which is used for generation of windshear and microburst alerts, will then increase from once every 5 minutes to once every minute.

2.2 Microburst and Windshear Detection Algorithm (WMDA)

The WMDA of TLC TDWR is developed by the Lincoln Laboratory, Massachusetts Institute of Technology (MIT). It identifies microburst and windshear features by finding out divergence segments from radial velocity data based on 0.6° elevation scan as well as the characteristics of upper flow features including formation of couplets indicating signs of rotation and downward motion of reflectivity cores suggesting the presence of downbursts (Merritt et al. 1989).

For BP TDWR, the WMDA is developed by the Japan Meteorological Agency (JMA). Only data from 0.6° elevation scan are used for windshear and microburst detection (Hamazu et al. 2000). The WMDA first searches for radial winds divergence segments, then validates the segments identified, and finally generates windshear or microburst features (Tse et al. 2019).

In real operation, a windshear alert is issued for shear magnitude of at least 15 knots (≥ 7.7 ms^{-1}). If it is of 30 knots or larger (≥ 15.4 ms^{-1}), a microburst alert would be issued.

2.3 Clutter removal

Both the TLC and BP TDWRs have included algorithms to remove quasi-stationary and moving objects such as ships, vehicles and cable cars near the HKIA.

The TLC TDWR uses a high-pass band filter to remove quasi-stationary clutters. For radar data with Doppler velocity between -2 ms^{-1} and +2 ms^{-1}, the associated signal is reduced by 55 dB (Shun 1995). Clutter polygon covering the Lantau Island is used to remove moving clutters such as vehicles on highways over the Lantau Island as well as eliminate multi-paths or sidelobe contamination over the area south of the HKIA (Shun and Lau 2000). Another clutter polygon is applied over the Castle Peak region to the north of the HKIA. In addition to clutter polygons, a point target removal algorithm is used to remove moving clutters over the seas that might be caused by high density of ship traffic or large bulk carriers.

For the BP TDWR, it uses clutter filter and clutter to signal ratio to remove quasi-stationary clutters (Tse 2016). An algorithm named as Moving Target Adaptive Rejection Map (MTARM) is employed to remove moving clutters. Details of MTARM can be found in Mitsubishi (2015). During optimization of the BP TDWR in 2014, signals from moving cable cars along part of the cable car ropeway were observed. MTARM was implemented in the BP TDWR to remove these signals (Figure 2). With the use MTARM, no clutter polygon was implemented in the BP TDWR.

3. BP TDWR suspicious observations

3.1 Anomalous windshear or microbursts alerts

On some occasions, the BP TDWR issued large windshear alerts (shear magnitude as high as 50 knots) which were apparently over-warning. This occurred particularly when generally southeasterlies prevailed over the HKIA and reverse flows were identified on the lee-side of the Lantau Island (Figure 3). This terrain-induced feature might sometimes extend to the HKIA ARENAs but the windshear magnitude was suspicious. Since the shear over the ARENA was much smaller, such large magnitude of windshear was seldom detected by the TLC TDWR. It is believed that the use of clutter polygons by the TLC TDWR was capable of suppressing alert area to extend to the return flows in the wakes of Lantau mountains and thus prevented the generation of anomalous windshear alerts.

3.2 Strong sidelobe return echoes

A narrow north-south oriented velocity feature with reflectivity generally less than 20 dBZ was sometimes observed over the seas at a near constant distance to the west of the BP TDWR (Figure 4). The feature might be

treated as a significant windshear event by the BP TDWR and a “suspicious alert” was issued. This was likely due to the detection of marine traffic by different sidelobes of the radar beam.

4. Experiment for improving the BP TDWR performance

In 2016-2018, HKO experimented the use of clutter polygons and adjustment of the BP TDWR WMDA parameters for mitigating the above problems mentioned in Section 3.

4.1 Data

The data used in the experiment included two tropical cyclone (TC) cases and four thunderstorm cases. These two types of weather scenarios might trigger the occurrences of windshear or microburst at the HKIA.

The two TC cases included TC Mujigae in 2015 and TC Pakhar in 2017. Mujigae posted great impact on the HKIA operation. Due to low-level windshear caused by Mujigae, there were 75 cases of missed approach for aircraft attempting to land at the HKIA. This was the highest since the opening of the HKIA in 1998. During the passage of TC Pakhar, more than 670 flights were cancelled or delayed. Four thunderstorm events in 2015 and 2016 were used. Details of the weather patterns triggering the thunderstorms are shown in Table 2.

4.2 Clutter polygons

The shapes of clutter polygons applied in the BP TDWR generally followed those of the Lantau Island and the mountains near the Castle Peak. Their sizes and shapes were further optimized based on their effectiveness in minimizing the anomalous windshear or microbursts alerts.

4.3 Adjustment of the BP TDWR WMDA parameters

Two parameters in the BP TDWR WMDA were adjusted in the experiment, namely, reflectivity threshold (Z_{min}) for determining divergence segments and the minimum area of windshear or microburst features (MB_{area}). It was expected that increasing Z_{min} would suppress the issuance of windshear/microburst alerts caused by sidelobe return due to marine vessels while reducing MB_{area} would prompt to higher chance of issuing windshear/microburst alerts. After numerous trials and testing, Z_{min} was adjusted from 5 dBZ to 10 dBZ while MB_{area} was tuned down from 3 km^2 to 1 km^2 which agreed better with the streak-like feature caused by the terrain of Lantau. Examples of alerts with areas of 3 km^2 and 1 km^2 were shown on Figure 3.

5. Methodology for verification

The effectiveness of windshear and microburst detection based on the following three different settings was compared:

(i) Setting A: original setting of the BP TDWR that has been in use since 2017;
(ii) Setting B: add clutter polygons over the Lantau Island and Castle Peak;
(iii) Setting C: adjust Z_{min} from 5 dBZ to 10 dBZ and MB_{area} from 3 km^2 to 1 km^2 in addition to adding clutter polygons.

Outputs of the settings were verified against pilot reports (PIREP) and data retrieved from the Quick Access Recorder (QAR) installed inside aircraft. The probability of detection (POD), false alarm ratio (FAR) and critical success index (CSI) were calculated based on the two TC cases.

For TCs Mujigae and Pakhar, 175 and 143 PIREP or QAR data were obtained for verification respectively. Only QAR data was used if both PIREP and QAR data were available. If there was a significant windshear (i.e. headwind change of at least 15 knots) based on PIREP or QAR at time (T) and the BP TDWR issued an alert in the 3-minute interval from T-3 to T, it was classified as a hit. Otherwise, it was a miss. If BP TDWR issued an alert but the PIREP did not support this, it was a false alarm.

6. Results

6.1 Reduction of anomalous windshear or microbursts alerts

The new settings were effective in reducing the microburst alert duration. For Pakhar, the duration of having microburst alert over runway ARENA (i.e., headwind loss of at least 30 knots) decreased from 7.1% in setting A to 5.3% in setting C. For Mujigae, the corresponding change was similar, from 7.2% to 5.2% (Table 3). Since flights would not land when microburst alerts are in effect, comparison of performance of microburst alert could not be conducted based on flight data.

The effect on windshear alert was also studied. Table 3 shows the runway alert duration for settings A and C. The duration for having windshear or microburst alerts over any one of the runway ARENAs during the event of Mujigae increased less than 1 % from 69.8% to 70.7% while there was little change for Pakhar (42.9% in setting A; 42.8% in setting C). This suggested the new setting still captured the windshear events.

For alert for the three different settings, the comparison results for TCs Mujigae and Pakhar are shown in Table 4 respectively. In the event of Mujigae, the POD using setting B was the same as that of setting A (78%) but slightly increased in setting C (80%). For Pakhar, the POD decreased from 70% in setting A to 63% in setting B but increased to 70% in setting C. For the FAR, it was 12% in setting A and slightly higher (13%) in setting C.

As setting C has similar POD as that of setting A and the microburst alert duration was shorter in setting C, the increase in windshear alert duration and FAR in setting C was small, setting C was considered as a suitable and desired setting.

The verification results based on the four thunderstorm cases are shown in Table 5. The duration of having microburst or windshear alerts over any runway ARENA were the same between setting A and setting C. However, there was significant difference for microburst alert duration in the thunderstorm case of 21 May 2016 (6.3% in setting A and only 0.6% in setting C). As discussed below under Section 7, this was not a pure thunderstorm case as it was assessed that the large magnitude of the microburst alerts were partly contributed by return flow in the wake of Lantau. Thus the reduction in microburst alert was considered a more realistic representation of the shear magnitude over the runway ARENA.

6.2 Minimizing sidelobe return echoes

For suspicious alerts due to strong sidelobe return of transiting marine vessels, Z_{min} was critical as the reflectivity of this feature was usually weak. With higher Z_{min}, the WMDA would become more stringent. On the other hand, if MB_{area} was reduced, a smaller feature would be regarded as a microburst or windshear and an alert would be issued.

In the experiment, it was found that adjusting Z_{min} from 5 dBZ to 10 dBZ and reducing MB_{area} from 3 km^2 to 1 km^2 could remove 25 out of 29 cases of suspicious alerts in the period from November 2016 to October 2017. An example is shown in Figure 5. In the original setting, a windshear alert of 25 knots was outputted by the WMDA in an area with reflectivity mostly less than 20 dBZ (Figure 5a). After adjusting both Z_{min} and MB_{area}, the windshear alert was removed (Figure 5b).

7. Discussion

The introduction of clutter polygon in the BP TDWR WMDA was found to affect if a windshear or microburst alert would be issued. Even if an alert was issued, the associated windshear magnitude would be different after applying clutter polygon.

Taking the case of Pakhar as an example, Figure 6 shows the WMDA outputs in the three different settings when an aircraft departing from the HKIA reported a headwind change from -20 knots (headwind loss of 10.3 ms^{-1}) to +15 knots (headwind gain of 7.7 ms^{-1}). In setting A, a windshear alert of 15 knots was issued as there were areas with opposite radial velocity, which were related to the terrain-induced reverse flows (Figure 6a). In setting B, no alert was issued as the number of divergence segments was reduced because

some of the areas with terrain-induced reverse flows at the lee-side of the Lantau Island were suppressed by clutter polygon (Figure 6b). As a result, the area enclosing divergence segments decreased to 2 km^2, less than the required threshold of 3 km^2. In setting C, a windshear alert of 15 knots covering a smaller area was issued (Figure 6c). In comparison, both settings A and C could capture the windshear event reported by PIREP while setting B failed to do so.

Moreover, it was assessed that setting C could reflect better the ARENA situation than setting A as exemplified by the case of 21 May 2016 (Figure 7). From Figure 7a, alerts were issued for four different areas under setting A. One with shear magnitude of 45 knots (23.2 ms^{-1}), one with 25 knots (12.9 ms^{-1}) and one with 20 knots (10.3 ms^{-1}). The one with 45 knots of windshear and alert area sticking near the northern coast of the Lantau Island was suspicious. It was thought that terrain-induced reverse flows in the wakes of the Lantau Island (green arrow in Figure 7a pointing those radial winds divergence segments that might likely be generated due to reverse flows) contributed to higher shear values and triggered the issue of the 45-knot microburst alert. With the use of clutter polygon in setting C, radar data near the wakes were masked. As a result, the 45-knot windshear alert was replaced by one with 20 knots (Figure 7b). It was considered to be more realistic to represent the shear value over the ARENA by examining the radial velocity over the ARENA.

The verification results based on thunderstorm cases show that the performances of settings A and C are comparable. But in some cases under setting C, the alert severity was reduced from microburst alerts to windshear alerts as the windshear magnitude was decreased. Also, for the case of 21 May 2016, the frequency of issuing microburst alert was reduced from 20 in setting A to 2 in setting C. Thus, the adoption of setting C could shorten the frequency of alerts with large shear magnitude in cases related to terrain-induced windshear. Checking of the case by human truthing supported that all the large shear magnitude alerts being removed in setting C were related to terrain-induced features. The two remaining cases were due to extension of the features to the runway ARENAs. More importantly, the problem of over-warning due to terrain-induced windshear could be mitigated as large shear magnitude could be reduced.

8. Conclusion

From the experiment, it was demonstrated that adding clutter polygons could improve the performance of the BP TDWR by reducing the issuance of anomalous windshear or microbursts alerts with large shear magnitudes. It was believed that the improvement was attributed to the suppression of terrain-induced reverse flows at the wakes of the Lantau mountains. By adjusting two of the BP TDWR WMDA parameters, Z_{min} and MB_{area}, the impact of marine traffic sidelobe returns that might trigger incorrect alerts could be effectively minimized.

HKO implemented the configuration of setting C in the BP TDWR WMDA in March 2018. To gain further insight of the spatial characteristics of terrain-induced windshear near the HKIA, spatial maps showing the distribution of windshear and microburst alerts issued by the BP TDWR were being compiled. Preliminary findings indicated that terrain-induced windshear was very prominent when southeasterly winds prevailed over Hong Kong (Figure 8a). Such feature was well illustrated during the influence of TC Mangkhut on 16-17 September 2018 where strong southeasterlies blowing across the mountains of the Lantau Island generated lines of vortex streaks that propagated downstream to the western side of the Lantau Island near the HKIA (Figure 8b).

9. Acknowledgements

The authors would like to thank Mr. Y.W. Lee, Joshua for compiling the spatial maps of windshear and microburst alerts and preparing the necessary for analysis.

10. References

Hamazu K., M. Ishihara, K. Hata, H. Hashiguchi, and S. Fukao, 2000: Development of low-level wind shear detection algorithm for the DRAW. *Institute of Electronics, Information and Communication IEICE*, **7**, 1067-1080. (in Japanese)

Hong Kong International Airport, 2019: Facts and Figures, HKIA at a Glance - Hong Kong International Airport, Accessed 28 July 2019, https://www.hongkongairport.com/iwov-resources/file/the-airport/hkia-at-a-glance/facts-figures/2018e.pdf

Hong Kong Observatory (HKO), 2010: *Windshear and Turbulence in Hong Kong - information for pilots*, 3rd edition, 2010, 36 pp. [Available online: https://www.hko.gov.hk/aviat/articles/WS-turb-booklet-eng-3rd.pdf]

Lau, S.Y., and C.M. Shun, 2002: Terrain-induced Wind Shear during the Passage of Typhoon Utor near Hong Kong in July 2001. *10th Conference on Mountain Meteorology and MAP meeting 2002*, Park City, Utah, USA, 17-21 June 2002.

Lee, O.S.M. and C.M. Shun, 1998: Optimization of the Terminal Doppler Weather Radar for the Hong Kong International Airport. *Proceedings of International Symposium on Electronic in the Air Transport Industry 98'*, Hong Kong, China, 18-19 November 1998.

Li, L., P.W. Chan and S.M. Tse, 2017: Observation and simulation of mountain wave trains in a tropical cyclone situation. *Mausam*, **68**, 253-260.

Merritt, M.W., D. Klingle-Wilson, and S.D. Campbell, 1989: Wind Shear Detection with Pencil-Beam Radars. *The Lincoln Laboratory Journal*, **2**, 483-510.

Mitsubishi Electric (H.K.) Ltd, 2015: *Technical Handbook, System User Manual, Software Documentation of Brothers Point Terminal Doppler Weather Radar System*.

Shun, C. M., 1995: "Implementation of a Terminal Doppler Weather Radar for the Chek Lap Kok Airport. *Symposium on Electronics in the Air Transport Industry (SEATI ' 95)*, Institution of Electrical Engineers, Hong Kong, 13-14 December 1995.

Shun, C. M., and P. W. Chan, 2008: Applications of an Infrared Doppler Lidar in Detection of Wind Shear. *Journal of Atmospheric and Oceanic Technology*, **25**, 637 - 655.

Shun, C.M., and S.Y. Lau, 2000: Terminal Doppler Weather Radar (TDWR) Observation of Atmospheric Flow over Complex Terrain during Tropical Cyclone Passages. *SPIE's Second International Asia-Pacific Symposium on Remote Sensing of the Atmosphere, Environment, and Space*, Sendai, Japan, 9-12 October 2000.

Shun, C.M., S.Y. Lau & O.S.M. Lee, 2003: Terminal Doppler Weather Radar Observation of Atmospheric Flow over Complex Terrain during Tropical Cyclone Passages. *Journal of Applied Meteorology*, **42**, 1697-1710.

Tse, S.M., 2016: Optimization of Terminal Doppler Weather Radar of Hong Kong International Airport for Microburst Detection. *9th European Conference on Radar in Meteorology and Hydrology*; Antalya, Turkey, 10-14 October 2016.

Tse, S.M., M. Hagio and Y. Maeda, 2019: Windshear Detection by Terminal Doppler Weather Radar during Tropical Cyclone Mujigae in 2015. *Meteorological Applications*, accepted on 9 March 2019, https://doi.org/10.1002/met.1789.

	TLC TDWR	BP TDWR
Antenna Diameter	7.6 m	7.9 m
Transmission Frequency	5,625 MHz	
Radar Beam Width	< 0.55 °	
Range Resolution	150 m	
Velocity Range	-80 ms^{-1} to 80 ms^{-1}	-73.6 ms^{-1} to 73.6 ms^{-1}
Peak Power	> 250 kW	

Table 1 Hardware specifications of the Hong Kong Observatory's Terminal Doppler Weather Radars (TDWR) at Tai Lam Chung (TLC) and Brothers Point (BP).

Case	Date/Period	Weather Pattern	Relevant Figure
1	24 May 2015	Squall Line	Figure 9a
2	29 July 2015	Convergence between south and southeasterlies	Figure 9b
3	21 May 2016	Surface trough	Figure 9c
4	9-10 July 2016	Thunderstorms triggered by intense insolation	Figure 9d

Table 2 Four thunderstorm cases employed for experimenting the impact of using clutter polygons and adjusting the Brothers Point (BP) Doppler Weather Radars (TDWR) parameters on the detection of windshear and microburst.

Alerts issued for the runway ARENAs	**Setting A**	**Setting C**
Mujigae (No. of total scan: 748)		
Windshear or microburst alert	522 (69.8%)	529 (70.7%)
Microburst alert	54 (7.2%)	39 (5.2%)
Pakhar (No. of total scan: 1,156)		
Windshear or microburst alert	496 (42.9%)	495 (42.8%)
Microburst alert	82 (7.1%)	61 (5.3%)

Table 3 Runway alert duration under settings A and C during the influences of tropical cyclones (TC) Mujigae and Pakhar.

Mujigae	Setting			**Pakhar**	Setting		
	A	B	C		A	B	C
Hit	134	133	136	Hit	71	64	71
Miss	37	38	35	Miss	30	37	30
False Alarm	1	1	0	False Alarm	10	10	11
POD (%)	78	78	80	POD (%)	70	63	70
FAR (%)	1	1	0	FAR (%)	12	14	13
CSI	0.78	0.77	0.80	CSI	0.64	0.58	0.63

Table 4 Comparison results of settings A, B, C for tropical cyclones Mujigae and Pakhar verified using PIREP and QAR data.

Alerts issued for the runway ARENAs	**Setting A**	**Setting C**
24 May 2015 (No. of total scan: 171)		
Windshear or microburst alert	23 (13.5%)	23 (13.5%)
Microburst alert	15 (8.8%)	15 (8.8%)
29 July 2015 (No. of total scan: 75)		
Windshear or microburst alert	22 (29.3%)	22 (29.3%)
Microburst alert	14 (18.7%)	15 (20.0%)
21 May 2016 (No. of total scan: 319)		
Windshear or microburst alert	97 (30.4%)	97 (30.4%)
Microburst alert	20 (6.3%)	2 (0.6%)
9-10 July 2016 (No. of total scan: 255)		
Windshear or microburst alert	48 (18.8%)	48 (18.8%)
Microburst alert	17 (6.7%)	17 (6.7%)

Table 5 Runway alert duration under settings A and C for the four thunderstorm cases occurred on 24 May 2015, 29 July 2015, 21 May 2016 and 9-10 July 2016 respectively.

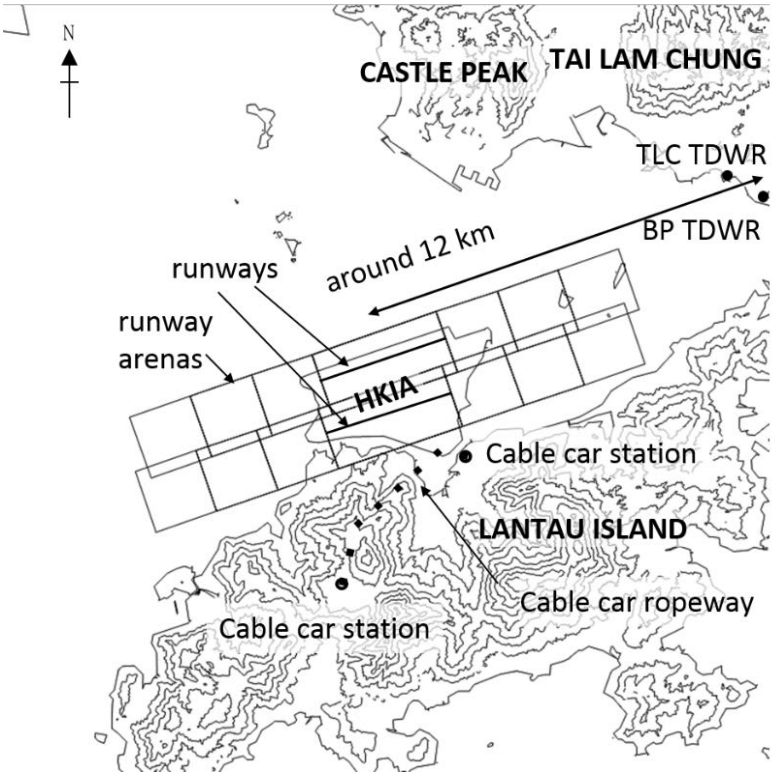

Figure 1 Location map of the HKIA. HKO operates two TDWRs at Tai Lam Chung (TLC) and Brothers Points (BP) respectively, about 12 km northeast of the central location of the HKIA. There are also two cable car stations over the Lantau Island to the south of the HKIA.

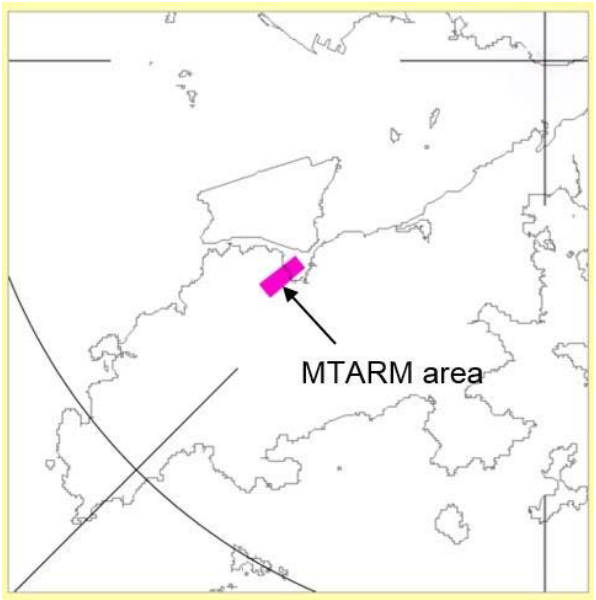

Figure 2 The Moving Target Adaptive Rejection Map (MTARM) algorithm implemented in the BP TDWR for removing moving clutters over the targeted area caused by moving cable cars (The purple strip shows the MTARM area).

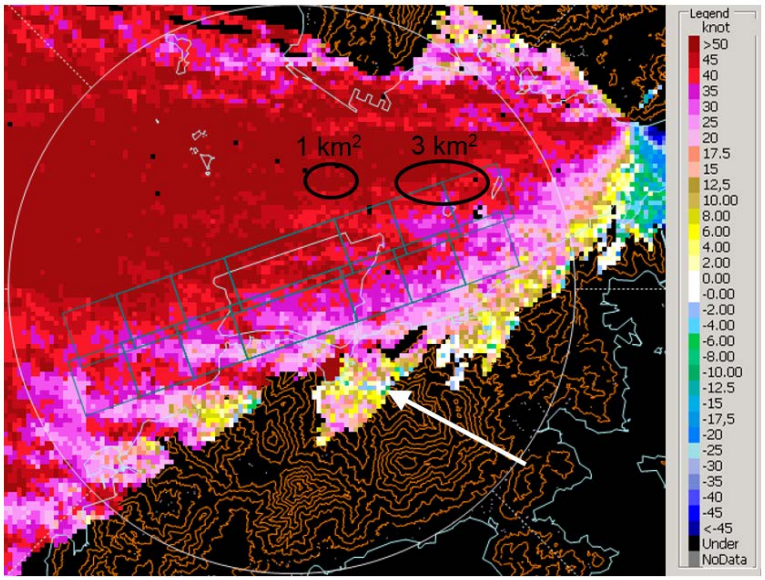

Figure 3 **Radial velocity image from HKO's BP TDWR taken at 7:03 Hong Kong Time (HKT) on 27 August 2017 showing the location of reverse flows (white arrow) [Warm and cold shadings represent radial velocity in knots (1 knot = 0.51 ms^{-1}) away and towards the BP TDWR respectively]. Examples of alerts with areas of 3 km^2 and 1 km^2 were shown on Figure 3. Please note that the alerts were for demonstrating the size only. They were NOT real alerts.**

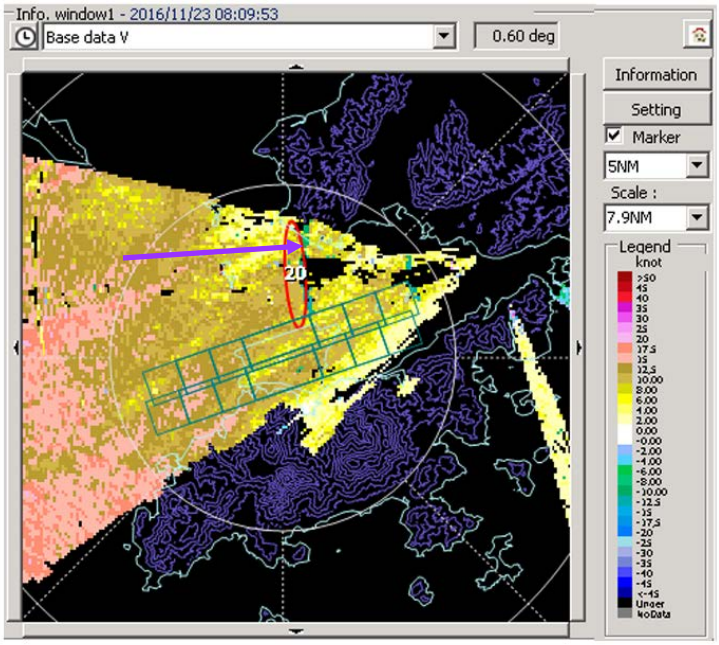

Figure 4 **Radial velocity image from HKO's BP TDWR taken at 8:09 HKT on 23 November 2016 showing a narrow north-south oriented velocity feature (purple arrow) likely caused by the strong sidelobe returns from marine vessels. [Warm and cold shadings represent radial velocity in knots (1 knot = 0.51 ms^{-1}) away and towards the BP TDWR respectively].**

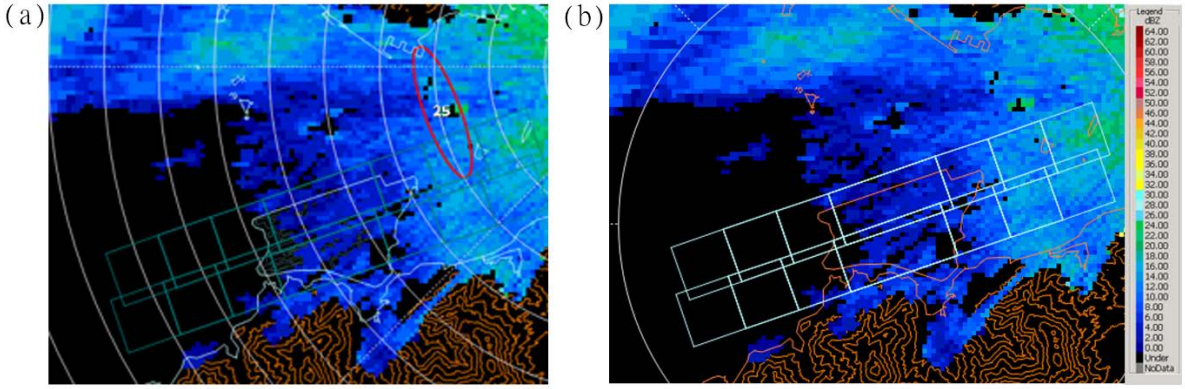

Figure 5 **Reflectivity images from HKO's BP TDWR taken at 09:02 HKT on 22 March 2017 under (a) Setting A: original BP TDWR setting. A windshear alert of 25 knots (red ellipse) with reflectivity mostly less than 20 dBZ was outputted by the BP TDWR WMDA; (b) the windshear alert was removed after adjusting WMDA parameters, Z_{min} from 5 dBZ to 10 dBZ, and MB_{area} from 3 km^2 to 1 km^2.**

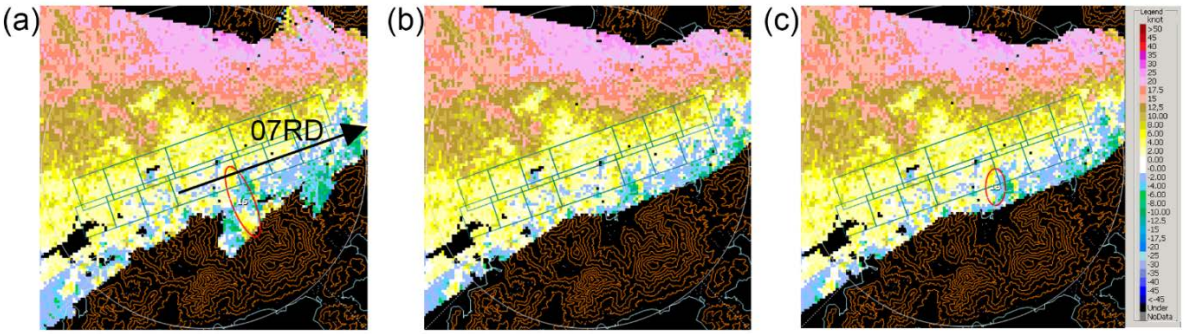

Figure 6 **Radial velocity images from HKO's BP TDWR based on 0.6° elevation scan taken on 27 August 2017 during the influence of TC Pakhar. An aircraft reported windshear when it departed from the runway 07R (taking off from the southwest to the northeast of the HKIA as shown in the black arrow [panel (a) on the leftmost]. (a) Setting A: the BP TDWR WMDA generated a windshear alert of 15 knots (red ellipse near the middle part of the runway); (b) Setting B: no alert was issued; (c) Setting C: a 15-knot windshear alert was issued (red ellipse near the middle part of the runway).**

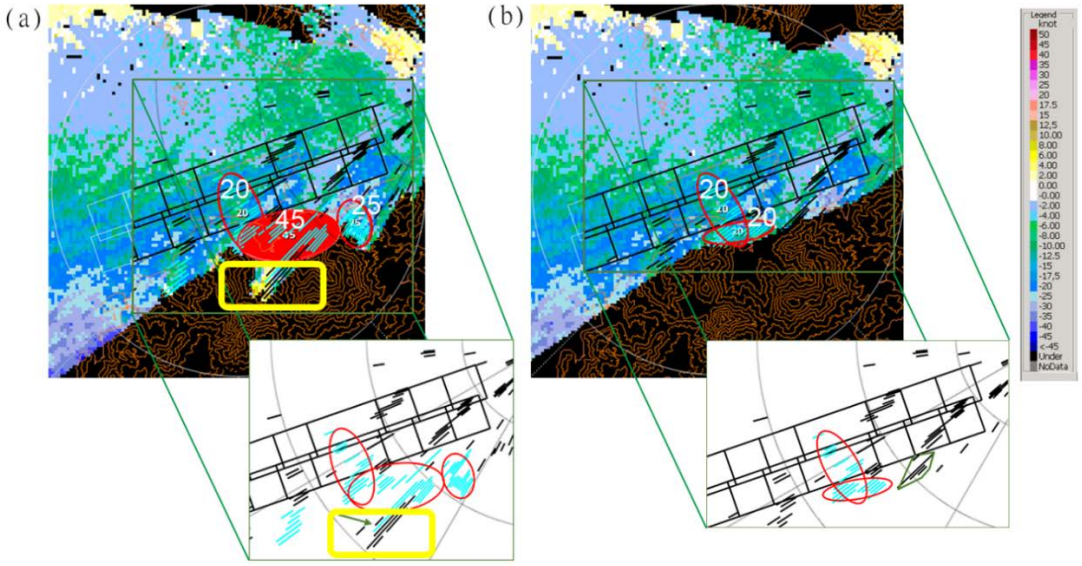

Figure 7 **Radial velocity images from HKO's BP TDWR taken at 04:57 HKT on 21 May 2016. Part of the runway ARENAs were zoomed (lower right) to show details of the radial winds divergence segments. Under the BP TDWR WMDA, those segments that would be included as valid or invalid windshear features were shown in cyan and black colours respectively; (a) Setting A: the 45-knot alert was believed to be caused by terrain-induced reverse flows in the wakes of the Lantau Island (green arrow pointed to the location of reverse flows enclosed by the yellow rectangle); (b) Setting C: with the use of clutter polygon masking radar data near the wakes, the number of segments and length of some segments in the wakes decreased. The 45-knot alert was replaced by a 20-knot alert.**

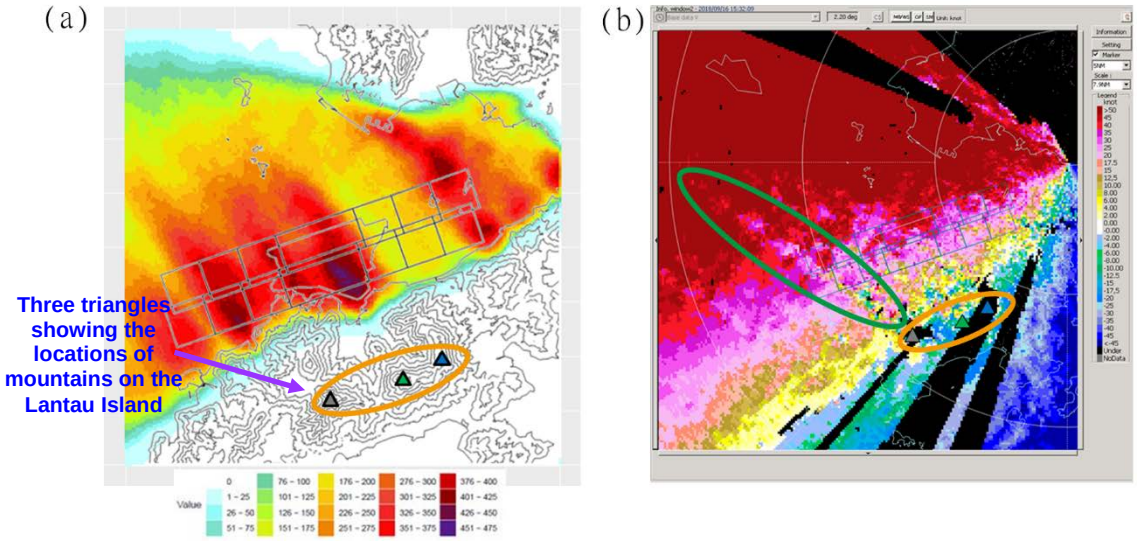

Figure 8 **Panel (a): Spatial density map of windshear and microburst alerts issued on 16-17 September 2018 under the influence of tropical cyclone Mangkhut; Panel (b): radial velocity image from HKO's BP TDWR based on 2.2° elevation scan taken at 15:32 HKT on 16 September 2018 (green ellipse showed one of the lines of vortex streaks. The three triangles within the orange ellipse showed the locations of high mountains over the Lantau Island).**

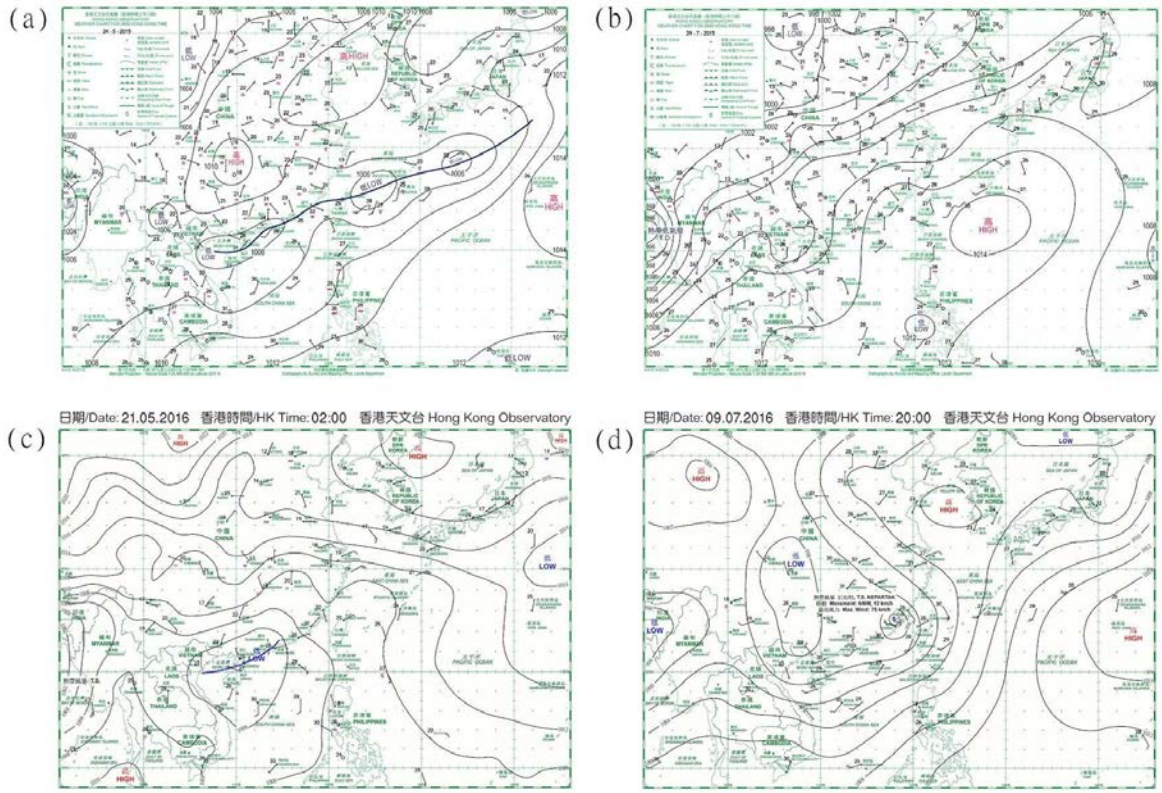

Figure 9 Surface pressure charts showing the weather patterns of the four thunderstorm cases; (a) A squall line associated with a surface trough on 24 May 2015; (b) Convergence between south and southeasterlies on 29 July 2015; (c) Surface trough with southwesterly winds prevailing over the HKIA on 21 May 2016; and (d) Thunderstorms triggered by intense insolation on 9 July 2016.